

RESEARCH LETTER

10.1029/2018GL079232

Key Points:

- Magnetosonic harmonic falling/rising frequency emissions were spaced by the local proton gyrofrequency
- Discrete magnetosonic emission lines crossed the proton gyrofrequency harmonics over a long period (up to 2 hr)
- Magnetosonic harmonic falling/rising frequency emissions primarily occurred in the dayside plasmatrough following intense substorms

Supporting Information:

- Supporting Information S1

Correspondence to:

Z. Su, szpe@mail.ustc.edu.cn

Citation:

Liu, N., Su, Z., Zheng, H., Wang, Y., & Wang, S. (2018). Magnetosonic harmonic falling and rising frequency emissions potentially generated by nonlinear wave-wave interactions in the Van Allen radiation belts. *Geophysical Research Letters*, 45. <https://doi.org/10.1029/2018GL079232>

Received 15 JUN 2018

Accepted 12 JUL 2018

Accepted article online 20 JUL 2018

Magnetosonic Harmonic Falling and Rising Frequency Emissions Potentially Generated by Nonlinear Wave-Wave Interactions in the Van Allen Radiation Belts

Nigang Liu^{1,2,3}, Zhenpeng Su^{1,2}, Huinan Zheng^{1,2}, Yuming Wang¹, and Shui Wang¹

¹CAS Key Laboratory of Geospace Environment, Department of Geophysics and Planetary Sciences, University of Science and Technology of China, Hefei, China, ²Collaborative Innovation Center of Astronautical Science and Technology, University of Science and Technology of China, Hefei, China, ³Mengcheng National Geophysical Observatory, School of Earth and Space Sciences, University of Science and Technology of China, Hefei, China

Abstract Magnetosonic waves play a potentially important role in the complex evolution of the radiation belt electrons. These waves typically appear as discrete emission lines along the proton gyrofrequency harmonics, consistent with the prediction of the local Bernstein mode instability of hot proton ring distributions. Magnetosonic waves are nearly dispersionless particularly at low harmonics and therefore have the roughly unchanged frequency time structures during the propagation. On the basis of Van Allen Probes observations, we here present the first report of magnetosonic harmonic falling and rising frequency emissions. They lasted for up to 2 hr and occurred primarily in the dayside plasmatrough following intense substorms. These harmonic emission lines were well spaced by the proton gyrofrequency but exhibited a clear falling (rising) frequency characteristic in a regime with the temporal increase (decrease) of the proton gyrofrequency harmonics. Such unexpected structures might be produced by the nonlinear interactions between the locally generated magnetosonic waves at the proton gyrofrequency harmonics and a constant frequency magnetosonic wave propagating away from the Earth.

Plain Language Summary Magnetosonic waves confined near the magnetospheric equator can scatter and accelerate the energetic electrons in the Van Allen radiation belts. Their precise generation and propagation processes remain the subjects of ongoing research and controversy. Here we report two new types of magnetosonic frequency-time structures: harmonic falling and rising frequency emissions. Available data and numerical estimations tend to support that these unusual structures were produced by the nonlinear interactions between the locally generated magnetosonic waves at the proton gyrofrequency harmonics and a constant frequency magnetosonic wave propagating away from the Earth. These unexpected frequency-time structures reported here bring new insights on the wave generation and propagation, which will be of high interest to the radiation belt and space plasma physics communities.

1. Introduction

Magnetosonic waves are the highly oblique low-frequency whistler-mode emissions confined near the magnetospheric equator (Gurnett, 1976; Russell et al., 1970; Santolík et al., 2002). These waves are frequently invoked to explain the complex evolution of energetic electrons in the Van Allen radiation belts (Li et al., 2016; Xiao et al., 2015; Yang et al., 2017; Zhao et al., 2014). The underlying physical processes could be Landau resonance (Horne et al., 2007), bounce resonance (Roberts & Schulz, 1968; Shprits, 2009) or transit-time scattering (Bortnik & Thorne, 2010). Hence, understanding and predicting the radiation belt dynamics require the knowledge of generation and propagation of magnetosonic waves.

The frequency-time structures of magnetosonic waves may provide key clues on their generation and propagation processes. In the high-resolution frequency-time spectrograms, magnetosonic waves often appear as discrete emission lines tracking the local proton gyrofrequency harmonics (Balikhin et al., 2015; Gary et al., 2010). This characteristic can be well explained by the local Bernstein mode instability of hot proton ring distributions (Boardsen et al., 1992; Curtis & Wu, 1979; Gary et al., 2010; Gulelmi et al., 1975; Horne et al., 2000;

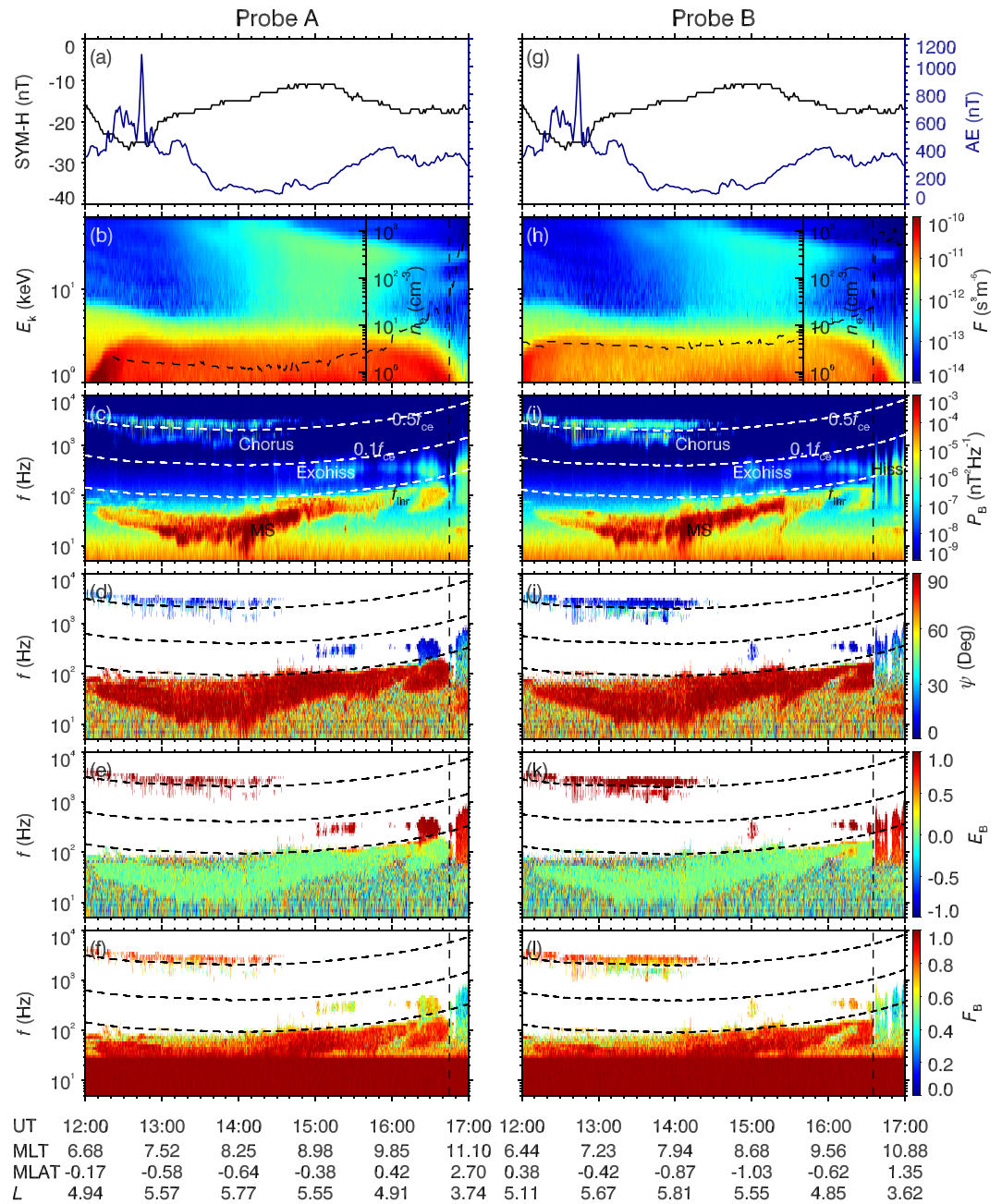


Figure 1. Overview of the magnetosonic wave event on 30 March 2016: (a, g) geomagnetic activity indices SYM-H and AE, (b, h) proton phase space density F and electron density n_e , (c, i) wave power spectral density P_B , (d, j) wave normal angle ψ , (e, k) wave ellipticity E_B (negative for left-hand polarized waves and positive for right-handed ones), and (f, l) wave planarity F_B . The vertical dashed lines mark the plasmopause location.

Meredith et al., 2008; Perraut et al., 1982; Yuan et al., 2017, 2018). Previous ray tracing simulations have suggested that magnetosonic waves are not trapped near the source region but propagate radially and azimuthally in the low-latitude region (Chen & Thorne, 2012; Horne & Miyoshi, 2016; Horne et al., 2000; Kasahara et al., 1994; Ma et al., 2014; Němec et al., 2013; Santolík et al., 2016). Because of the nearly dispersionless characteristic particularly at low harmonics (Boardsen et al., 2014), their frequency-time structures change little during the propagation (Su et al., 2017). Far away from the source, magnetosonic emission lines can cross the local proton gyrofrequency harmonics (Santolík, Pickett, Gurnett, Maksimovic, et al., 2002, 2016) and even occur below the local proton gyrofrequency (e.g., Li et al., 2016; Yang et al., 2017).

In this letter, we show two new types of magnetosonic frequency-time structures observed by the Van Allen Probes mission (Mauk et al., 2013). The magnetosonic emission lines exhibited a clear falling (rising) frequency characteristic in a regime with the temporal increase (decrease) of the proton gyrofrequency harmonics, and surprisingly, the adjacent emission lines were spaced by the local proton gyrofrequency over a long-time period (up to 2 hr). Investigation of these unexpected frequency-time structures may bring new insights on the magnetosonic wave generation and propagation.

2. Data and Method

The Van Allen Probes (Mauk et al., 2013) is a twin-spacecraft mission in the near-equatorial orbits with perigees $\sim 0.1 R_E$ and apogees $\sim 6 R_E$. These orbits allow Van Allen Probes to well detect the magnetosonic waves in the inner magnetosphere. We obtain the wave spectral matrices from the Electric and Magnetic Field Instrument and Integrated Science (EMFISIS) suite (Kletzing et al., 2013). The on-board spectral matrices of the waveform receiver (WFR) of the EMFISIS Waves instrument cover the frequency range from ~ 5 Hz to 10 kHz with a relatively low resolution in frequency and time. To analyze the high-resolution wave spectral matrices, we perform the fast Fourier transform (FFT) on the local magnetic fields measured by the fluxgate magnetometer (MAG) of the EMFISIS suite. The sampling rate of magnetic fields is 64 Hz, leading to the upper frequency limit of 32 Hz of the high-resolution spectra. Using the singular value decomposition method (Santolík, Pickett, Gurnett, & Storey, 2002, 2003), we infer the wave normal angle and the planarity and ellipticity of wave polarization from those spectral matrices. Based on observations of the upper hybrid resonance frequency by the high-frequency receiver of the EMFISIS Waves instrument, we can estimate the background electron density (Kurth et al., 2014). The Helium Oxygen Proton Electron (HOPE) instrument (Funsten et al., 2013) and the Magnetic Electron Ion Spectrometer (MagEIS; Blake et al., 2013) of the Energetic Particle, Composition and Thermal Plasma Suite (ECT; Spence et al., 2013) and the Radiation Belt Storm Probes Ion Composition Experiment (RBSPICE; Mitchell et al., 2013) can measure the hot proton fluxes. The proton energy ranges covered by the HOPE, MagEIS, and RBSPICE instruments are about 0.001–60, 60–1,200, and 40–600 keV, respectively. The HOPE and RBSPICE data usually exhibit a mismatch around 50 keV, and because of the ion implant damage, the MagEIS data at lower energy channels are highly noisy since March 2013. In this study, we mainly use the HOPE data (0.1–60 keV) to evaluate the linear growth rates (Chen et al., 2010; Kennel, 1966) of the hot proton Bernstein mode instability. The linear instability code has been developed by Su et al. (2018) and Liu et al. (2018). More details on the data fitting (De Boer, 1977; Reinsch, 1967) and the potential influence of >60 -keV protons on the wave growth rates are discussed in the supporting information (Text S1 and Figures S1 and S2).

3. Representative Events

Figure 1 gives an overview of the magnetosonic wave event on 30 March 2016. The magnetosphere exhibited strong substorms (maximum AE $> 1,000$ nT) but no storms (SYM-H > -30 nT) in the time range of interest. The twin Van Allen Probes with a separation distance of $\sim 2,000$ km were traveling in the dayside ($6 < |MLT| < 12$) near-equatorial ($|MLAT| < 3^\circ$) radiation belt ($3.6 < L < 5.1$). They detected hiss waves (0.05–1 kHz) in the high-density plasmasphere but chorus (around $0.5f_{ce}$), exohiss (around $0.1f_{ce}$), and magnetosonic waves (below f_{hr}) in the low-density plasmatrough. These magnetosonic waves had quasi-perpendicular wave vector ($\psi > 80^\circ$), nearly linear polarization ($E_B \approx 0$) and high planarity ($F_B > 0.7$), consistent with early observations (e.g., Horne et al., 2007; Perraut et al., 1982). There were proton ring distributions around 10–50 keV in the plasmatrough, favoring the local generation/amplification of magnetosonic waves (Balikhin et al., 2015; Boardsen et al., 1992; Curtis & Wu, 1979; Gary et al., 2010; Gulelmi et al., 1975; Horne et al., 2000; Meredith et al., 2008; Perraut et al., 1982). Figure 2 plots the high-resolution magnetosonic wave characteristics. Initially, magnetosonic waves peaked around fifth–eighth proton gyrofrequency harmonics. Around 13:52 UT, the enhancement of proton rings obviously intensified the magnetosonic waves and enlarged their occurrence frequency range. Subsequently, these magnetosonic emission lines split into two groups: one tracking the temporally increasing proton gyrofrequency harmonics and the other exhibiting the falling frequency feature. Both groups had the same characteristics of wave normal angle, polarity, and planarity. The former group became unobservable after 14:50 UT, while the latter group lasted for about 1 hr and even extended below the proton gyrofrequency.

Figure 3 displays another magnetosonic wave event on 11 November 2015. The magnetosphere exhibited some weak storm (SYM-H ≈ -35 nT) and intense substorm (AE $\approx 1,000$ nT) activities in the time range

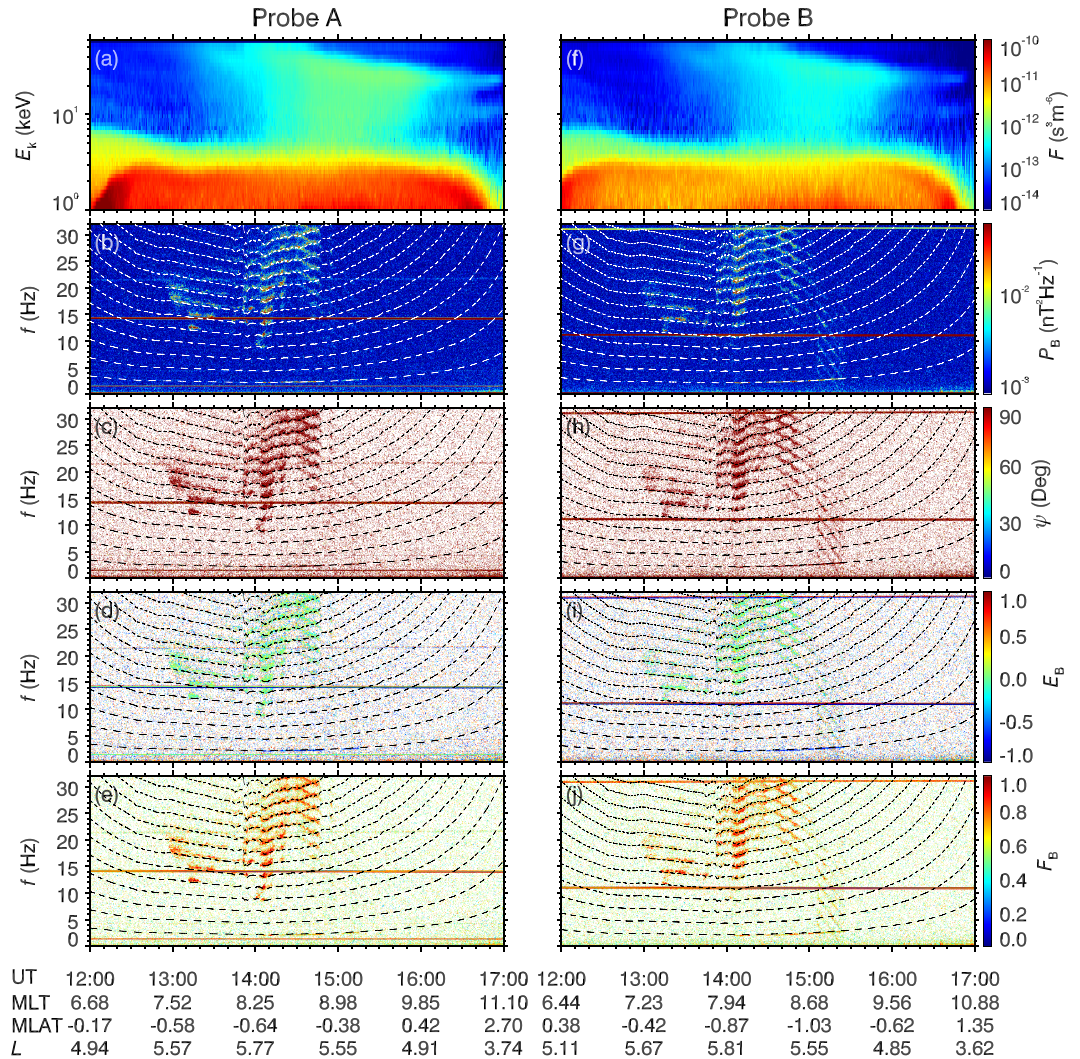


Figure 2. Hot proton distributions and high-resolution wave characteristics (<32 Hz) on 30 March 2016: (a, f) proton phase space density F , (b, g) wave power spectral density P_B , (c, h) wave normal angle ψ , (d, i) wave ellipticity E_B (negative for left-hand polarized waves and positive for right-handed ones), and (e, j) wave planarity F_B . The dashed lines represent the equatorial proton gyrofrequency harmonics.

of interest. Although the proton ring distributions were restricted outside the plasmapause ($L \approx 3.1$), the magnetosonic signals arose both inside and outside the plasmasphere. As discussed in the previous studies (Chen & Thorne, 2012; Ma et al., 2014; Su et al., 2017), the magnetosonic waves might be generated in the plasmatrough and then propagated into the plasmasphere. The most intense magnetosonic waves were detected by the Van Allen Probe B during 03:00–04:00 UT ($3.6 < L < 4.9$, $10.3 < |\text{MLT}| < 11.8$, $|\text{MLAT}| < 0.8^\circ$). In the high-resolution spectrogram, these waves can be divided into two groups: one without clear structures and the other with discrete rising frequency elements in a regime with temporally decreasing proton gyrofrequency harmonics. These harmonic rising frequency emission lines started below the proton gyrofrequency and lasted for about 1 hr.

4. Discussions

4.1. Wave Generation and Propagation

In Figure 4, we compare the observed magnetosonic spectrograms to the linear convective growth rates of whistler waves with normal angle $\psi = 89.5^\circ$. As illustrated in previous theoretical and numerical works (Boardsen et al., 1992; Chen et al., 2010; Gulelmi et al., 1975; Perraut et al., 1982), the Bernstein mode instability of hot protons (Figures S3 and S4) occurs around the proton gyrofrequency harmonics. For the 30 March

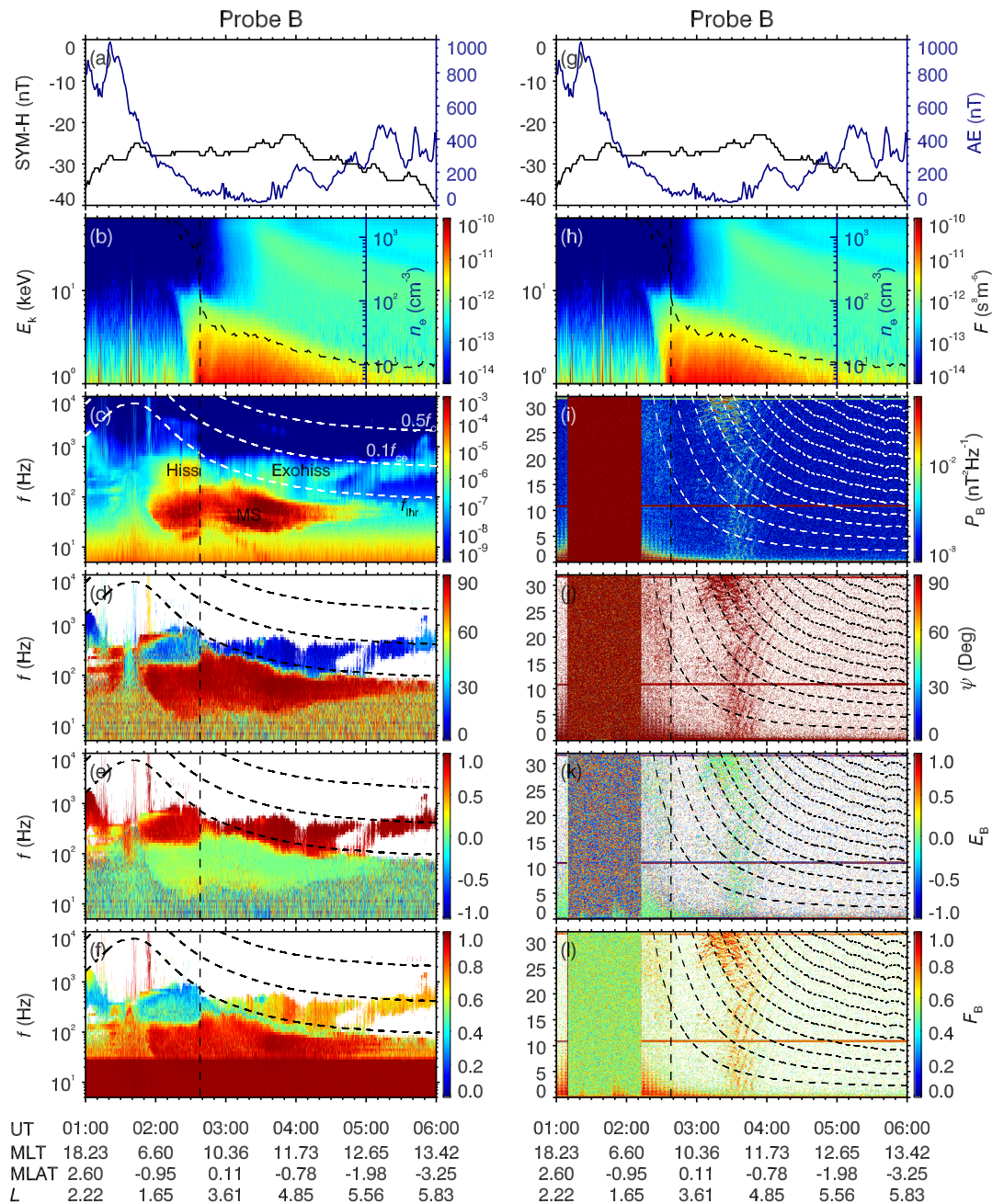


Figure 3. Overview of the magnetosonic wave event on 11 November 2015: (a, g) geomagnetic activity indices SYM-H and AE, (b, h) proton phase space density F and electron density n_e , (c) low-resolution and (i) high-resolution wave power spectral density P_B , (d, j) wave normal angle ψ , (e, k) wave ellipticity E_B (negative for left-hand polarized waves and positive for right-handed ones), (f, l) wave planarity F_B . The vertical dashed lines mark the plasmapause location.

2016 event, the modeled instability is able to qualitatively explain the temporal variation of the usual magnetosonic waves tracking the proton gyrofrequency harmonics. Throughout the event, the wave growth is allowed primarily in the frequency range >5 Hz, consistent with the wave observations (Figures 4a and 4b). The growth rates roughly peak during 14:00–14:30 UT, corresponding to the emergence of the most intense magnetosonic waves. These peak growth rates are close to the suggested threshold 10^{-6} m^{-1} for observable magnetosonic waves (Chen et al., 2010). After 15:00 UT, the growth rates decrease to less than 10^{-8} m^{-1} , responsible for the disappearance of the usual magnetosonic waves below 30 Hz. However, these linear convective growth rates present no observable correlation to the rising frequency magnetosonic waves.

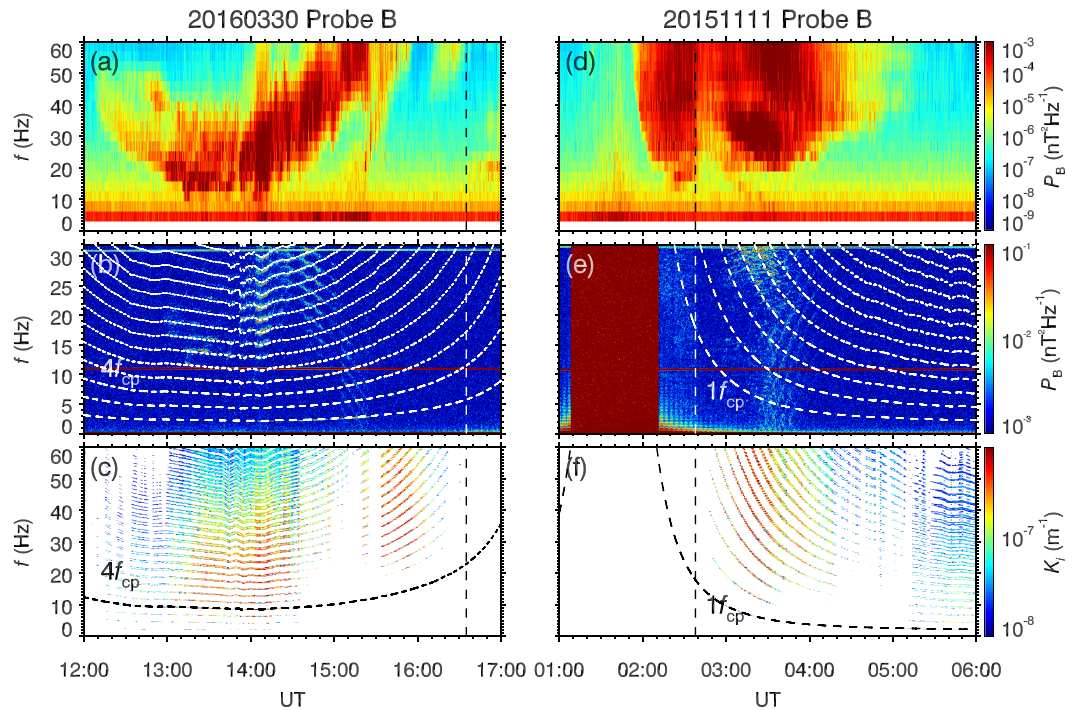


Figure 4. Bernstein mode instability for magnetosonic waves during the events on 30 March 2016 and 11 November 2015: (a, d) low-resolution and (b, e) high-resolution wave power spectral density P_B ; (c, f) convective growth rate K_i for whistler waves with normal angle $\psi = 89.5^\circ$. The vertical dashed lines mark the plasmapause location.

For the 11 November 2015 event, the model reproduces the occurrence of maximum wave power during 03:00–04:00 UT but cannot explain the noisy or rising frequency characteristics of magnetosonic waves.

In Figure 5, we re-render the wave spectra to isolate the magnetosonic emission lines. For the 30 March 2016 event, one can identify the falling frequency emission lines during the time period from 14:25 UT to 15:25 UT (with an observable weakening around 15:00 UT). Surprisingly, the adjacent emission lines were well spaced by the proton gyrofrequency throughout the event. In contrast to the increase of emission line spacing by about 1.28 times within 57 min (14:25–15:22 UT), the wave frequency (marked by white arrow) decreased by about 3.3 times. A quite similar situation existed in the 11 November 2015 event. The rising frequency emission lines were still spaced by the local proton gyrofrequency from 03:32 to 04:07 UT. Corresponding to the 1.49 times decrease in the emission line spacing, the wave frequency (marked by white arrow) increased by about 7.0 times. Near the source region, the wave frequency is usually expected to be proportional to the emission line spacing in the framework of the linear Bernstein mode instability of hot protons (Figure 4). The magnetosonic waves at low harmonics are nearly dispersionless (Boardsen et al., 2014), and their frequency-time structures should change little during the propagation (Su et al., 2017). Such opposite variations in the wave frequency and the emission line spacing are difficult to be explained by the wave propagation process (Chen & Thorne, 2012; Horne & Miyoshi, 2016; Horne et al., 2000; Kasahara et al., 1994; Ma et al., 2014; Santolík et al., 2016).

In the nonlinear framework, two plausible explanations may be given for these unusual wave frequency-time structures. One possibility is the nonlinear wave-particle interaction, which had been proposed to explain the fine structures of chorus, hiss, and electromagnetic ion cyclotron waves (Omura et al., 2008, 2010, 2015; Pickett et al., 2010; Su et al., 2018; Summers et al., 2014). However, the time duration and the spatial coverage of a magnetosonic emission line were observed to reach 1 hr and $1 R_E$. It is questionable whether the coherent nonlinear growth of waves can act on such a large spatiotemporal scale. Another possibility is the nonlinear wave-wave interaction, which had been proposed to explain the deviation of magnetosonic emission lines from the proton gyrofrequency harmonics (Perraut et al., 1982). The corresponding resonance conditions are written as

$$\omega_0 = \omega_1 + \omega_2, \quad (1)$$

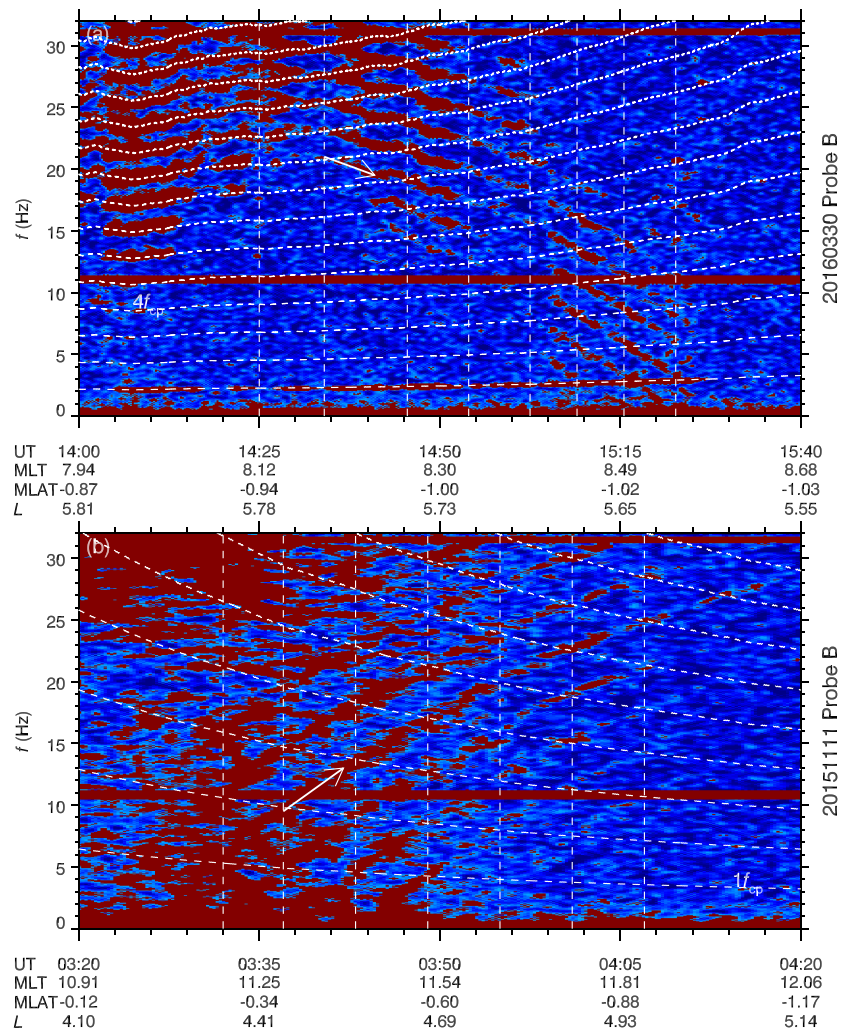


Figure 5. Rerendered wave spectra on (a) 30 March 2016 and (b) 11 November 2015. The equatorial proton gyrofrequency harmonic lines and the vertical lines are overplotted to help identify the temporal evolution of wave frequency and emission line spacing.

$$\mathbf{k}_0 = \mathbf{k}_1 + \mathbf{k}_2, \quad (2)$$

where ω_i and \mathbf{k}_i are the angular frequency and the wave vector of i th wave. The interactions between the usual harmonic magnetosonic waves ($\omega_1 = N_1 f_{cp}$) and a constant frequency (ω_0) magnetosonic wave could generate the magnetosonic harmonic falling/rising frequency emission lines (ω_2). As shown in Figure 6, for an arbitrary emission line ω_2 , one can find a reasonable N_1 to obtain a nearly constant ω_0 from the resonance condition (1) throughout the event. The expected pump waves (ω_0 and ω_1) occurred above >32 Hz, which were observable only in the low-resolution spectra. The low-frequency pump wave ω_1 was likely excited by the local proton Bernstein mode instability (Figure 4), and the high-frequency pump wave ω_0 might be generated at inner magnetic shells and propagate away from the Earth. The intensities of two waves ω_1 and ω_2 are found to vary synchronously throughout the events. For the event on 30 March 2016, corresponding to the weakening of the falling frequency emission lines ω_2 mentioned before (Figure 5a), there was a clear dip in the wave ω_1 power around 15:00 UT. For the event on 11 November 2015, both waves ω_1 and ω_2 showed decreasing power with time. These calculations and observations tend to support the action of the nonlinear wave-wave interactions.

As discussed above, the magnetosonic harmonic falling and rising frequency emissions were likely generated by the same physical process (nonlinear wave-wave interaction; Perraut et al., 1982) over a wide spatial region. The frequencies of newly generated waves $\omega_2 = \omega_0 - \omega_1$ are expected to vary oppositely

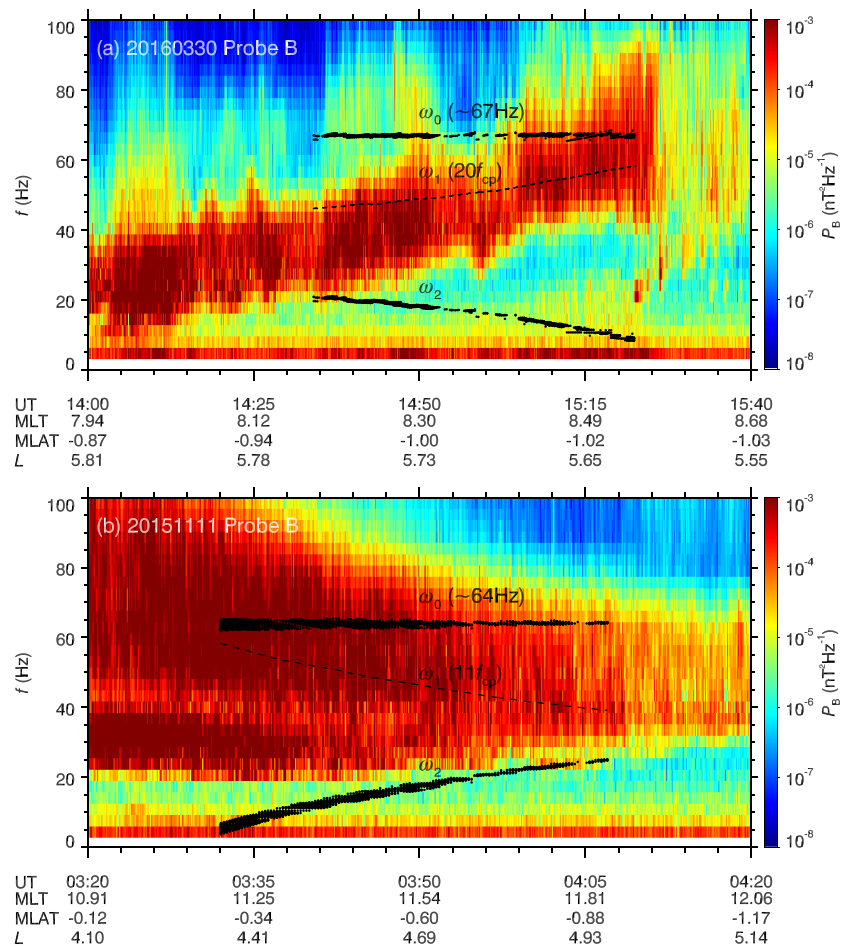


Figure 6. Sketch of wave-wave interactions for the events on (a) 30 March 2016 and (b) 11 November 2015. The background image is the low-resolution wave power spectral density P_B in frequency range 0–100 Hz. The emission lines ω_2 (marked by white arrows in Figure 5) are composed of the isolated intense signals; the emission lines ω_1 at the proton gyrofrequency harmonics are given after some tests; the emission lines ω_0 are calculated from the resonance condition (1).

to the proton gyrofrequency harmonics ω_1 . During the inbound pass with the increase of proton gyrofrequency harmonics, the spacecraft would observe the falling frequency emission lines. On the contrary, the outbound pass would allow the observations of the rising frequency emission lines. These unusual magnetosonic emissions reported here are essentially different from the quasiperiodic (~ 1 – 3 min) rising tone magnetosonic waves in the low-resolution data (Boardsen et al., 2014; Fu et al., 2014) or the rising tone magnetosonic waves associated with the substorm proton injections (Su et al., 2017). As illustrated by Némec et al. (2015), those rising tones in the low-resolution data were still composed of usual harmonic emission lines along the proton gyrofrequency harmonics in the high-resolution spectrogram and might be attributed to the proton Bernstein mode instability modulated by the compressional magnetic field pulsations. Following the substorm proton injection, the Van Allen Probes did observe the rising frequency magnetosonic emission lines with a duration of ~ 20 min in the high-resolution spectrogram (Su et al., 2017), which were likely caused by the earthward movement of wave source. However, their emission line spacing varied synchronously with the wave frequency and exhibited no correlation with the proton gyrofrequency at the probes (Figure S5).

4.2. Spatiotemporal Distribution

Based on the Van Allen Probes data from September 2012 to August 2017, we have manually identified 20 magnetosonic harmonic falling/rising frequency emissions (Table S1 and Figures S6–S25) and plotted their spatiotemporal distributions in Figure 7. It can be found that the falling frequency emissions had much higher occurrence rate (16/20) than the rising frequency emissions (4/20). The longest and shortest durations

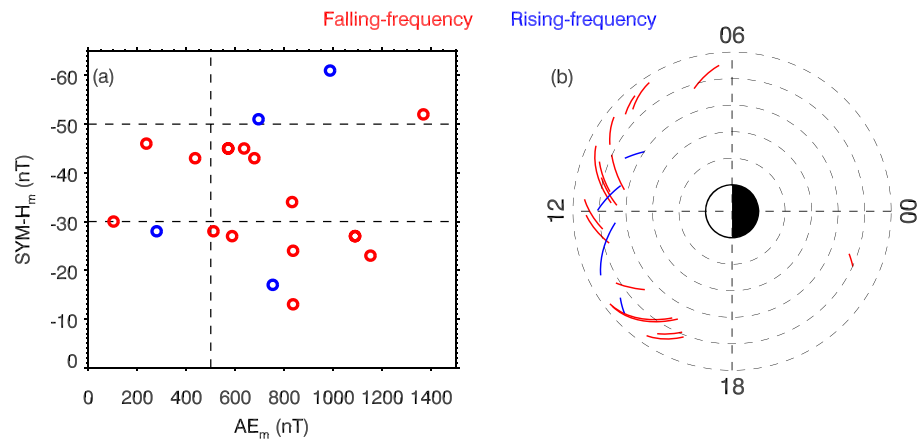


Figure 7. Spatiotemporal distributions of magnetosonic harmonic falling (red) and rising (blue) frequency emissions observed by the Van Allen Probes in the time period from September 2012 to August 2017: (a) dependence on AE_m (maximum AE in the preceding 3 hr) and SYM-H_m (minimum SYM-H in the preceding 12 hr); (b) dependence on L and magnetic local time.

of these waves were ~ 2 hr (Figure S6) and ~ 20 min (Figure S12). For all these events, the emission line spacing equaled the proton gyrofrequency and exhibited a temporal variation opposite to that of the wave frequency. Wave structures like those shown in Figure S5 have been excluded in our statics. Most of these waves were observed in the dayside low-density plasmatrough following intense substorms ($AE > 500$ nT), generally consistent with previous statistical studies of magnetosonic waves on the basis of low-resolution data (Boardsen et al., 2016; Hrbáčková et al., 2015; Kim & Shprits, 2017; Ma et al., 2013; Meredith et al., 2008; Němec et al., 2015; Shprits et al., 2013). Magnetosonic waves can be destabilized by the substorm-injected hot protons (Boardsen et al., 1992; Curtis & Wu, 1979; Gary et al., 2010; Gulelmi et al., 1975; Horne et al., 2000; Meredith et al., 2008; Yuan et al., 2017, 2018) and propagate over a broad region (Chen & Thorne, 2012; Horne & Miyoshi, 2016; Kasahara et al., 1994; Ma et al., 2014; Němec et al., 2013; Santolík et al., 2016; Su et al., 2017), allowing the subsequent nonlinear wave-wave interactions (Perraut et al., 1982). However, different from previous statistics (Yang et al., 2017), the occurrence of these unusual magnetosonic waves did not show any clear dependence on the geomagnetic storm activity.

In contrast to the frequent observations of magnetosonic waves by the WFR instrument, a quite limited number of magnetosonic harmonic falling/rising frequency events were found in the MAG-FFT data. The main reasons may be the stringent requirement for the generation of these unusual structures and the much higher detection threshold of MAG-FFT ($\sim 10^{-3}$ nT²/Hz) than that of WFR ($\sim 10^{-9}$ nT²/Hz). All the falling/rising frequency structures of MAG-FFT had some correlated magnetosonic signals of WFR at frequencies of tens of hertz, but at frequencies of $\sim < 10$ Hz, the WFR signals with relatively strong noise and low frequency resolution often exhibited no clear correspondence to the falling/rising frequency structures of MAG-FFT (Figure 6).

5. Summary

On the basis of Van Allen Probes observations, we have reported two new types of magnetosonic frequency-time structures: harmonic falling and rising frequency emissions. Over a long time period of up to 2 hr, these magnetosonic emission lines were well spaced by the proton gyrofrequency at the probes but exhibited a clear falling (rising) frequency characteristic in a regime with the temporal increase (decrease) of the proton gyrofrequency harmonics. From September 2012 to August 2017, we have found 20 events of magnetosonic harmonic falling (16) and rising (4) frequency emissions. They primarily occurred in the dayside plasmatrough following intense substorms, generally consistent with previous statistical studies of magnetosonic waves on the basis of low-resolution wave spectra (Boardsen et al., 2016; Hrbáčková et al., 2015; Kim & Shprits, 2017; Ma et al., 2013; Meredith et al., 2008; Němec et al., 2015; Shprits et al., 2013). Such magnetosonic frequency-time structures are difficult to be explained by the linear Bernstein mode instability or the subsequent propagation process alone (Balikhin et al., 2015; Gary et al., 2010; Santolík et al., 2002, 2016; Su et al., 2017). Available data and numerical estimations tend to support that these unusual structures were caused by the nonlinear interactions (Perraut et al., 1982) between the locally generated magnetosonic waves at the proton gyrofrequency harmonics and an outward propagating magnetosonic wave with a constant frequency. In future, more theoretical and observational studies are required to examine this scenario.

Acknowledgments

We acknowledge EMFISIS, ECT, and RBSPICE teams for the use of Van Allen Probes data. Data are available from the following websites: <http://emfisis.physics.uiowa.edu/Flight/>, http://www.rbbsp-ect.lanl.gov/data_pub/, <http://rbspice.ftccs.com/Data.html>, and <http://www.space.umn.edu/rbbspew-data/>. This work was supported by the National Natural Science Foundation of China grants 41631071, 41774170, 41274174, 41174125, 41131065, 41421063, 41231066, and 41304134, the Chinese Academy of Sciences grants KZCX2-EW-QN510 and KZZD-EW-01-4, the CAS Key Research Program of Frontier Sciences grant QYZDB-SSW-DQC015, the National Key Basic Research Special Foundation of China grant 2011CB811403, and the Fundamental Research Funds for the Central Universities WK2080000077.

References

- Balikhin, M. A., Shprits, Y. Y., Walker, S. N., Chen, L., Cornilleau-Wehrin, N., Dandouras, I., et al. (2015). Observations of discrete harmonics emerging from equatorial noise. *Nature Communications*, 6, 7703. <https://doi.org/10.1038/ncomms8703>
- Blake, J. B., Carranza, P. A., Claudepierre, S. G., Clemmons, J. H., Crain, W. R., Dotan, Y., et al. (2013). The Magnetic Electron Ion Spectrometer (MagEIS) instruments aboard the Radiation Belt Storm Probes (RBSP) spacecraft. *Space Science Reviews*, 179, 383–421. <https://doi.org/10.1007/s11214-013-9991-8>
- Boardsen, S. A., Gallagher, D. L., Gurnett, D. A., Peterson, W. K., & Green, J. L. (1992). Funnel-shaped, low-frequency equatorial waves. *Journal of Geophysical Research*, 97, 14,967–14,976. <https://doi.org/10.1029/92JA00827>
- Boardsen, S. A., Hospodarsky, G. B., Kletzing, C. A., Engebretson, M. J., Pfaff, R. F., Wygant, J. R., et al. (2016). Survey of the frequency dependent latitudinal distribution of the fast magnetosonic wave mode from Van Allen Probes Electric and Magnetic Field Instrument and Integrated Science waveform receiver plasma wave analysis. *Journal of Geophysical Research: Space Physics*, 121, 2902–2921. <https://doi.org/10.1002/2015JA021844>
- Boardsen, S. A., Hospodarsky, G. B., Kletzing, C. A., Pfaff, R. F., Kurth, W. S., Wygant, J. R., & MacDonald, E. A. (2014). Van Allen Probe observations of periodic rising frequencies of the fast magnetosonic mode. *Geophysical Research Letters*, 41, 8161–8168. <https://doi.org/10.1002/2014GL062020>
- Bortnik, J., & Thorne, R. M. (2010). Transit time scattering of energetic electrons due to equatorially confined magnetosonic waves. *Journal of Geophysical Research*, 115, A07213. <https://doi.org/10.1029/2010JA015283>
- Chen, L., & Thorne, R. M. (2012). Perpendicular propagation of magnetosonic waves. *Geophysical Research Letters*, 39, L14102. <https://doi.org/10.1029/2012GL052485>
- Chen, L., Thorne, R. M., Jordanova, V. K., & Horne, R. B. (2010). Global simulation of magnetosonic wave instability in the storm time magnetosphere. *Journal of Geophysical Research*, 115, A11222. <https://doi.org/10.1029/2010JA015707>
- Curtis, S. A., & Wu, C. S. (1979). Gyroharmonic emissions induced by energetic ions in the equatorial plasmasphere. *Journal of Geophysical Research*, 84, 2597–2607. <https://doi.org/10.1029/JA084iA06p02597>
- De Boor, C. (1977). Package for calculating with B-splines. *SIAM Journal on Numerical Analysis*, 14(3), 441–472.
- Fu, H. S., Cao, J. B., Zhima, Z., Khotyaintsev, Y. V., Angelopoulos, V., Santolik, O., et al. (2014). First observation of rising-tone magnetosonic waves. *Geophysical Research Letters*, 41, 7419–7426. <https://doi.org/10.1002/2014GL061867>
- Funsten, H. O., Skoug, R. M., Guthrie, A. A., MacDonald, E. A., Baldoonado, J. R., Harper, R. W., et al. (2013). Helium, oxygen, proton, and electron (HOPE) mass spectrometer for the radiation belt storm probes mission. *Space Science Reviews*, 179, 423–484. <https://doi.org/10.1007/s11214-013-9968-7>
- Gary, S. P., Liu, K., Winske, D., & Denton, R. E. (2010). Ion Bernstein instability in the terrestrial magnetosphere: Linear dispersion theory. *Journal of Geophysical Research*, 115, A12209. <https://doi.org/10.1029/2010JA015965>
- Gulelmi, A. V., Klaine, B. I., & Potapov, A. S. (1975). Excitation of magnetosonic waves with discrete spectrum in the equatorial vicinity of the plasmopause. *Planetary and Space Science*, 23, 279–286. [https://doi.org/10.1016/0032-0633\(75\)90133-6](https://doi.org/10.1016/0032-0633(75)90133-6)
- Gurnett, D. A. (1976). Plasma wave interactions with energetic ions near the magnetic equator. *Journal of Geophysical Research*, 81, 2765–2770. <https://doi.org/10.1029/JA081i016p02765>
- Horne, R. B., & Miyoshi, Y. (2016). Propagation and linear mode conversion of magnetosonic and electromagnetic ion cyclotron waves in the radiation belts. *Geophysical Research Letters*, 43, 10,034–10,039. <https://doi.org/10.1002/2016GL070216>
- Horne, R. B., Thorne, R. M., Glauert, S. A., Meredith, N. P., Pokhotelov, D., & Santolik, O. (2007). Electron acceleration in the Van Allen radiation belts by fast magnetosonic waves. *Geophysical Research Letters*, 34, L17107. <https://doi.org/10.1029/2007GL030267>
- Horne, R. B., Wheeler, G. V., & Alleyne, H. S. C. K. (2000). Proton and electron heating by radially propagating fast magnetosonic waves. *Journal of Geophysical Research*, 105, 27,597–27,610. <https://doi.org/10.1029/2000JA000018>
- Hrbáčková, Z., Santolik, O., Němec, F., Macušová, E., & Cornilleau-Wehrin, N. (2015). Systematic analysis of occurrence of equatorial noise emissions using 10 years of data from the Cluster mission. *Journal of Geophysical Research: Space Physics*, 120, 1007–1021. <https://doi.org/10.1002/2014JA020268>
- Kasahara, Y., Kenmochi, H., & Kimura, I. (1994). Propagation characteristics of the ELF emissions observed by the satellite Akebono in the magnetic equatorial region. *Radio Science*, 29, 751–767. <https://doi.org/10.1029/94RS00445>
- Kennel, C. (1966). Low-frequency whistler mode. *Physics of Fluids*, 9, 2190–2202. <https://doi.org/10.1063/1.1761588>
- Kim, K.-C., & Shprits, Y. (2017). Dependence of the amplitude of magnetosonic waves on the solar wind and AE index using Van Allen Probes. *Journal of Geophysical Research: Space Physics*, 122, 6022–6034. <https://doi.org/10.1002/2017JA024094>
- Kletzing, C. A., Kurth, W. S., Acuna, M., MacDowall, R. J., Torbert, R. B., Averkamp, T., et al. (2013). The Electric and Magnetic Field Instrument Suite and Integrated Science (EMFISIS) on RBSP. *Space Science Reviews*, 179, 127–181. <https://doi.org/10.1007/s11214-013-9993-6>
- Kurth, W. S., Pascuale, S. D., Faden, J. B., Kletzing, C. A., Hospodarsky, G. B., Thaller, S., & Wygant, J. R. (2014). Electron densities inferred from plasma wave spectra obtained by the Waves instrument on Van Allen Probes. *Journal of Geophysical Research: Space Physics*, 120, 904–914. <https://doi.org/10.1002/2014JA020857>
- Li, J., Ni, B., Ma, Q., Xie, L., Pu, Z., Fu, S., et al. (2016). Formation of energetic electron butterfly distributions by magnetosonic waves via Landau resonance. *Geophysical Research Letters*, 43, 3009–3016. <https://doi.org/10.1002/2016GL067853>
- Liu, N., Su, Z., Zheng, H., Wang, Y., & Wang, S. (2018). Prompt disappearance and emergence of radiation belt magnetosonic waves induced by solar wind dynamic pressure variations. *Geophysical Research Letters*, 45, 585–594. <https://doi.org/10.1002/2017GL076382>
- Ma, Q., Li, W., Chen, L., Thorne, R. M., Kletzing, C. A., Kurth, W. S., et al. (2014). The trapping of equatorial magnetosonic waves in the Earth's outer plasmasphere. *Geophysical Research Letters*, 41, 6307–6313. <https://doi.org/10.1002/2014GL061414>
- Ma, Q., Li, W., Thorne, R. M., & Angelopoulos, V. (2013). Global distribution of equatorial magnetosonic waves observed by THEMIS. *Geophysical Research Letters*, 40, 1895–1901. <https://doi.org/10.1002/grl.50434>
- Mauk, B. H., Fox, N. J., Kanekal, S. G., Kessel, R. L., Sibeck, D. G., & Ukhorskiy, A. (2013). Science objectives and rationale for the radiation belt storm probes mission. *Space Science Reviews*, 179, 3–27. <https://doi.org/10.1007/s11214-012-9908-y>
- Meredith, N. P., Horne, R. B., & Anderson, R. R. (2008). Survey of magnetosonic waves and proton ring distributions in the Earth's inner magnetosphere. *Journal of Geophysical Research*, 113, A06213. <https://doi.org/10.1029/2007JA012975>
- Mitchell, D. G., Lanzerotti, L. J., Kim, C. K., Stokes, M., Ho, G., Cooper, S., et al. (2013). Radiation Belt Storm Probes Ion Composition Experiment (RBSPICE). *Space Science Reviews*, 179, 263–308. <https://doi.org/10.1007/s11214-013-9965-x>
- Němec, F., Santolik, O., Hrbáčková, Z., Pickett, J. S., & Cornilleau-Wehrin, N. (2015). Equatorial noise emissions with quasiperiodic modulation of wave intensity. *Journal of Geophysical Research: Space Physics*, 120, 2649–2661. <https://doi.org/10.1002/2014JA020816>
- Němec, F., Santolik, O., Pickett, J. S., Hrbáčková, Z., & Cornilleau-Wehrin, N. (2013). Azimuthal directions of equatorial noise propagation determined using 10 years of data from the Cluster spacecraft. *Journal of Geophysical Research: Space Physics*, 118, 7160–7169. <https://doi.org/10.1002/2013JA019373>

- Omura, Y., Katoh, Y., & Summers, D. (2008). Theory and simulation of the generation of whistler-mode chorus. *Journal of Geophysical Research*, *113*, A04223. <https://doi.org/10.1029/2007JA012622>
- Omura, Y., Nakamura, S., Kletzing, C. A., Summers, D., & Hikishima, M. (2015). Nonlinear wave growth theory of coherent hiss emissions in the plasmasphere. *Journal of Geophysical Research: Space Physics*, *120*, 7642–7657. <https://doi.org/10.1002/2015JA021520>
- Omura, Y., Pickett, J., Grison, B., Santolik, O., Dandouras, I., Engebretson, M., et al. (2010). Theory and observation of electromagnetic ion cyclotron triggered emissions in the magnetosphere. *Journal of Geophysical Research*, *115*, A07234. <https://doi.org/10.1029/2010JA015300>
- Perraut, S., Roux, A., Robert, P., Gendrin, R., Sauvaud, J.-A., Bosqued, J.-M., et al. (1982). A systematic study of ULF waves above F_{H+} from GEOS 1 and 2 measurements and their relationships with proton ring distributions. *Journal of Geophysical Research*, *87*, 6219–6236. <https://doi.org/10.1029/JA087iA08p06219>
- Pickett, J. S., Grison, B., Omura, Y., Engebretson, M. J., Dandouras, I., Masson, A., et al. (2010). Cluster observations of EMIC triggered emissions in association with Pc1 waves near Earth's plasmapause. *Geophysical Research Letter*, *37*, L09104. <https://doi.org/10.1029/2010GL042648>
- Reinsch, C. H. (1967). Smoothing by spline functions. *Numerical Mathematics*, *10*(3), 177–183.
- Roberts, C. S., & Schulz, M. (1968). Bounce resonant scattering of particles trapped in the Earth's magnetic field. *Journal of Geophysical Research*, *73*, 7361–7376. <https://doi.org/10.1029/JA073i023p07361>
- Russell, C. T., Holzer, R. E., & Smith, E. J. (1970). OGO 3 observations of ELF noise in the magnetosphere. 2. The nature of the equatorial noise. *Journal of Geophysical Research*, *75*, 755–768. <https://doi.org/10.1029/JA075i004p00755>
- Santolik, O., Parrot, M., & Lefeuvre, F. (2003). Singular value decomposition methods for wave propagation analysis. *Radio Science*, *38*(1), 1010. <https://doi.org/10.1029/2000RS002523>
- Santolik, O., Parrot, M., & Nèmec, F. (2016). Propagation of equatorial noise to low altitudes: Decoupling from the magnetosonic mode. *Geophysical Research Letter*, *43*, 6694–6704. <https://doi.org/10.1002/2016GL069582>
- Santolik, O., Pickett, J. S., Gurnett, D. A., Maksimovic, M., & Cornilleau-Wehrlin, N. (2002). Spatiotemporal variability and propagation of equatorial noise observed by Cluster. *Journal of Geophysical Research*, *107*(A12), 1495. <https://doi.org/10.1029/2001JA009159>
- Santolik, O., Pickett, J. S., Gurnett, D. A., & Storey, L. R. O. (2002). Magnetic component of narrowband ion cyclotron waves in the auroral zone. *Journal of Geophysical Research*, *107*(A12), 1444. <https://doi.org/10.1029/2001JA000146>
- Shprits, Y. Y. (2009). Potential waves for pitch-angle scattering of near-equatorially mirroring energetic electrons due to the violation of the second adiabatic invariant. *Geophysical Research Letter*, *36*, L12106. <https://doi.org/10.1029/2009GL038322>
- Shprits, Y. Y., Runov, A., & Ni, B. (2013). Gyro-resonant scattering of radiation belt electrons during the solar minimum by fast magnetosonic waves. *Journal of Geophysical Research: Space Physics*, *118*, 648–652. <https://doi.org/10.1002/jgra.50108>
- Spence, H. E., Reeves, G. D., Baker, D. N., Blake, J. B., Bolton, M., Bourdarie, S., et al. (2013). Science goals and overview of the radiation belt storm probes (RBSP) energetic particle, composition, and thermal plasma (ECT) suite on NASA's Van Allen Probes mission. *Space Science Reviews*, *179*, 311–336. <https://doi.org/10.1007/s11214-013-0007-5>
- Su, Z., Liu, N., Zheng, H., Wang, Y., & Wang, S. (2018). Large-amplitude extremely low frequency hiss waves in plasmaspheric plumes. *Geophysical Research Letter*, *45*, 565–577. <https://doi.org/10.1002/2017GL076754>
- Su, Z., Wang, G., Liu, N., Zheng, H., Wang, Y., & Wang, S. (2017). Direct observation of generation and propagation of magnetosonic waves following substorm injection. *Geophysical Research Letter*, *44*, 7587–7597. <https://doi.org/10.1002/2017GL074362>
- Summers, D., Omura, Y., Nakamura, S., & Kletzing, C. A. (2014). Fine structure of plasmaspheric hiss. *Journal of Geophysical Research: Space Physics*, *119*, 9134–9149. <https://doi.org/10.1002/2014JA020437>
- Xiao, F., Yang, C., Su, Z., Zhou, Q., He, Z., He, Y., et al. (2015). Wave-driven butterfly distribution of Van Allen belt relativistic electrons. *Nature Communications*, *6*, 8590. <https://doi.org/10.1038/ncomms9590>
- Yang, C., Su, Z., Xiao, F., Zheng, H., Wang, Y., Wang, S., et al. (2017). A positive correlation between energetic electron butterfly distributions and magnetosonic waves in the radiation belt slot region. *Geophysical Research Letter*, *44*, 3980–3990. <https://doi.org/10.1002/2017GL073116>
- Yuan, Z., Yu, X., Huang, S., Qiao, Z., Yao, F., & Funsten, H. O. (2018). Cold ion heating by magnetosonic waves in a density cavity of the plasmasphere. *Journal of Geophysical Research: Space Physics*, *123*, 1242–1250. <https://doi.org/10.1002/2017JA024919>
- Yuan, Z., Yu, X., Huang, S., Wang, D., & Funsten, H. O. (2017). In situ observations of magnetosonic waves modulated by background plasma density. *Geophysical Research Letter*, *44*, 7628–7633. <https://doi.org/10.1002/2017GL074681>
- Zhao, H., Li, X., Blake, J. B., Fennell, J. F., Claudepierre, S. G., Baker, D. N., et al. (2014). Peculiar pitch angle distribution of relativistic electrons in the inner radiation belt and slot region. *Geophysical Research Letter*, *41*, 2250–2257. <https://doi.org/10.1002/2014GL059725>